

pubs.acs.org/JPCC Article

Probing Heterodimer and Multiadsorbate Hydrocarbon Adsorption Trends in the MFI Framework

Elsa Koninckx, Pavlo Kostetskyy, and Linda J. Broadbelt*



Cite This: J. Phys. Chem. C 2022, 126, 13894-13904



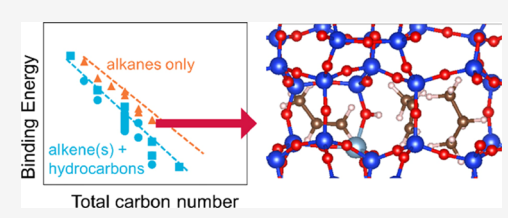
ACCESS I

Metrics & More

Article Recommendations

Supporting Information

ABSTRACT: Acidic zeolites are highly versatile and industrially relevant catalysts and molecular sieves with numerous applications. Zeolites can be functionalized with a range of possible active sites, including Brønsted acid functionalities. Three-dimensional zeolite frameworks such as MFI have been a popular choice in petrochemical applications, such as isomerization, cracking, and oligomerization chemistries. Adsorption is generally considered to be a coverage-dependent phenomenon. Additional complications arise when the adsorbate mixture is not homogeneous and contains multiple molecular identities, resulting in preferential



adsorption of certain adsorbate classes at the expense of others. The extent of preference is important in hydrocarbon processing and separations, typically characterized by heterogeneous mixtures of varying molecular identity, size, and shape. Following our previous investigation into the trends of monomer and homodimer adsorption, we quantify heterodimer and multiadsorbate adsorption energies of various combinations of hydrocarbons (alkenes and alkanes) in HZSM-5. We examine heterodimer adsorption trends at three tetrahedral positions in the MFI framework, contrast homodimer and heterodimer adsorption behavior, examine the effect of branching, and investigate the adsorption of trimers, tetramers, and higher. Linear scaling relations between binding energies and molecular size are identified and reported. Alkenes capable of pi-bonding generally adsorb stronger than alkane-only hydrocarbon mixtures. Dependence on the degree of branching as well as the carbon number can provide better estimates for adsorption energies. Additionally, the linear scaling trends reported can likely be extrapolated to larger adsorbates or many more adsorbates in proximity to a single acid site (high loadings). These correlations provide higher accuracy and better understanding of adsorption in mixed-feed separations and bimolecular catalytic reactions.

■ INTRODUCTION

Zeolites are porous aluminosilicates with repeating micropore structures. There are diverse classes of zeolites, characterized by the framework pore structure, that can accommodate a wide variety of adsorbates while remaining stable under various reaction conditions, making them widely applicable. Zeolites are commonly used as commercial adsorbents and catalysts; ^{1,2} more specifically, zeolites are used for selective adsorption in water purification and gas separations and as catalysts in petrochemical processing reactions. ^{3–5}

Replacing Si⁴⁺ with an Al³⁺ ion and compensating H⁺ species into the silica framework results in intraframework Brønsted acid (BA) sites. Catalytic conversion of hydrocarbons over acidic zeolites is applied in large petrochemical refining processes, including catalytic cracking, hydrocracking, isomerization, and oligomerization. Additionally, acidic zeolites are being used to adsorb impurities, such as sulfur-containing compounds.

The chemical composition of the framework and the number of BA sites are dependent on the synthesis conditions. In most cases, total loading of framework alumina is reported as a silica to aluminum ratio (Si/Al), which correlates with the acid site concentration and porosity. There are 12 uniquely possible tetrahedral positions (T-sites) for the Al substitution of Si in the MFI (ZSM-5) framework. Several investigations have sought to identify the most stable and catalytically relevant positions.

Deprotonation energy studies done by Jones and Iglesia suggested that the location of the isolated Al is not significant in zeolites. Likewise, Zhang et al. and Alvarado-Swaisgood et al. found that, for all 12 T-sites, the differences in energies were small (<15 kJ mol⁻¹) such that Al may substitute into any site under suitable conditions. 9,10

There have been a number of multiscale, computational studies examining the sorption of saturated and unsaturated hydrocarbons in porous aluminosilicates, focusing on adsorbate identity and size, pore topology, acid site concentration, operating pressure, and presence of inorganic cations, among others. Particular attention has been paid to the accuracy of calculated thermodynamic quantities such as enthalpy and entropy—important considerations that contribute to systematic error propagation in these systems include anharmonicity of vibrational modes, 12–16 translational and rotational motion of the adsorbate, 17–20 long-range interactions such as van der

Received: April 15, 2022 Revised: July 14, 2022 Published: August 1, 2022





Waals (vdW) and dispersion, ^{21,22} and the interadsorbate interactions across partial pressure ranges. ^{17,23–25} With sufficient corrections, the accuracy of calculated values can be at the level of chemical accuracy, although care must be taken in the assumptions made. Furthermore, the corrections to the calculated energies can be system-specific and variables such as pore topology and size play a significant role. In the case of atomistic simulations, these errors can be exacerbated for mixtures of adsorbates of differing identities, structures, and sizes.

The adsorption of hydrocarbon mixtures is a common practice in the petrochemical industry, with a number of possible species present. The coadsorption events are characterized by competition for access to the active site, with the alkene species showing a greater preference over the alkanes. However, the adsorption of molecular dimers of varying size and molecular identity can produce results counter to the typical alkene preference, as the sum of weak interactions of alkanes and zeolite pore walls can exceed the BA site— π bond interactions.

In the past, acid or proton site positions have been difficult to characterize and analyze, in turn making the understanding of the adsorbate location and adsorption energies difficult to quantify.²⁶ Rather, density functional theory (DFT) has been used to understand this phenomenon, and DFT techniques have advanced along with computational ability.²⁷ Grimme et al. managed to quantify this and reported that the mean absolute deviations for the D3(BJ) potentials with the Perdew, Burke, and Ernzerhof (PBE) functional, which are used in this study, were calculated to be ~0.5 kcal/mol. 28,29 Electronic structure calculations quantifying the coadsorption of dimers of different sizes and identities have been scarce, with stochastic simulations of molecular adsorption dominating in the literature.^{30–32} However, the zeolite-adsorbate and adsorbate-adsorbate interactions are accounted for by forcefield potentials that require tuning and do not capture the fundamental physics of interactions.

There have been previous DFT studies specifically investigating the adsorption of alkanes and alkenes into acidic zeolite frameworks. Göltl and Hafner modeled the adsorption of short alkanes in protonated chabazite. They found weak binding with the acid site, such that only vdW interactions between the alkane and zeolite remained. 15 Most notably, De Moor et al.'s studies compare physisorption and chemisorption energies between alkenes and alkanes across common zeolite frameworks, such as MFI, BEA, and FAU, and are often summarized with linear correlation coefficients between energies and the carbon number. $^{33-35}$ Throughout these hydrocarbon adsorption investigations, energies are only reported for a single adsorbed hydrocarbon; however, molecular adsorption in zeolites is coverage dependent, and coadsorption events are required for processes such as catalytic oligomerization and large-volume separations. In our previous work, we quantified monomer and homodimer adsorption trends in the siliceous and acidic MFI framework.30

For this work, we further expand our study of dimer adsorption by analyzing how mixtures of alkanes and alkenes adsorb into acidic MFI (HZSM-5). Using periodic electronic structure calculations, we report physisorption electronic energies, enthalpies, and free energies of adsorption in H-ZSM-5 for heterodimer mixtures of ethene and ethane to hexene and hexanes on various acidic T-site locations. Additionally, linear and branched heterodimer adsorption trends are quantified and compared as well as an analysis of multiadsorbate

adsorption trends. The results include linear correlations for heterodimer adsorption energy as a function of total carbon number. The correlations reported can improve the accuracy of multiadsorption energies in common mixed hydrocarbon feeds to better understand selective separations and model catalytic reactions.

COMPUTATIONAL METHODS

Fully periodic DFT calculations were performed using the Vienna ab initio software package (VASP). The geometry optimizations, energy cut offs, vibrational frequency calculations, and initial MFI (ZSM-5) framework structure are the same as those found in our previous work.³⁶ The projector augmented wave method was used to construct plane-wave functionals with an energy cutoff of 400 eV. 37,38 The Brillouin zone was sampled at the Γ -point for all calculations. All calculations used the generalized gradient approximation of PBE.²⁴ The DFT-D3 empirical correction with Becke and Johnson damping (D3BJ) was used to consider dispersion interactions. Geometries were optimized in two steps to maximize chemical accuracy with computational efficiency: (i) structures were optimized with conjugate-gradient algorithm (IBRION = 2) keeping energy variations between SCF iterations <10-6 eV, forces were computed with a fast Fourier transform grid of 2× the default energy cutoff (PREC = ACCURATE in VASP), and structures were relaxed until the maximum force on any atom was <0.05 eV/Å; (ii) the structures were reoptimized with a quasi-Newton algorithm (IBRION = 1), and structures were relaxed until wave functions converged to $<10^{-6}$ eV and maximum force on any atom to <0.01 eV/Å.

The MFI (ZSM-5) unit cell framework structure was obtained from the database of the International Zeolite Association, with unit cell parameters a = 20.090 Å, b = 19.738 Å, c = 13.142 Å, and $a = b = c = 90.0^{\circ}$. The unit cell was optimized allowing for the relaxation of atomic positions, unit cell shape, and volume (ISIF = 3) with an energy cutoff of 800 eV. This optimization resulted in a minor increase of unit cell parameters a = 20.443 Å, b = 20.176 Å, and c = 13.581 Å.

There are 12 unique tetrahedral positions available for Al substitution in the MFI framework. While studies have reported small energy differences in the acid position, the T7, T9, and T12 sites are often reiterated as being the lowest energy or most favorable sites for Al substitution; for this reason, these initial three sites were chosen for further investigation. 8–10 The T7, T9, and T12 positions were specifically selected to be at an intersection of straight and sinusoidal channels, allowing for adsorbates to access the large, open void at this intersection, aiding in adsorption (Figure 1).

Binding energies (BE) of adsorbates were calculated in reference to adsorbates and zeolites at infinite separation, according to eq 1, where $\Delta E_{\rm complex}$ is the energy of the adsorbate complex, $\Delta E_{\rm zeolite}$ is the energy of the empty zeolite framework, and $\Delta E_{\rm adsorbate,i}$ is the gas-phase energy of the adsorbate.

$$\Delta BE = \Delta E_{\text{complex}} - \Delta E_{\text{zeolite}} - \sum \Delta E_{\text{adsorbate},i}$$
 (1)

Zero-point vibrational energies ($\Delta E_{\rm ZPE}$), enthalpies (ΔH), and free energies (ΔG) were approximated by vibrational frequency calculations with a fixed displacement method for all gas-phase and adsorbed species. Framework Si and O atoms not bound to the Al atom were fixed in the framework during frequency calculations. The Al, bonded O, and adsorbate molecules were considered for vibrations, such that translations

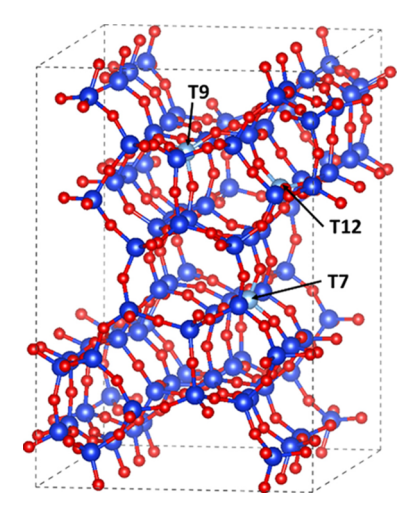


Figure 1. Graphical representation of T7, T9, and T12 positions (light blue) with surrounding oxygen (red) and silicon (blue) for the MFI framework.

and rotations were frustrated. Enthalpies and free energies were approximated using statistical thermodynamics, where ΔE_0 is the total electronic energy of the system, $\Delta E_{\rm ZPE}$ is the zero-point vibrational energy, vib is the vibrational contribution, trans is the translational contribution, and rot is the rotational contribution to state functions.

$$\Delta H = \Delta E_0 + \Delta E_{\text{ZPE}} + \Delta H_{\text{vib}} + \Delta H_{\text{trans}} + \Delta H_{\text{rot}}$$
 (2)

$$\Delta G = \Delta E_0 + \Delta E_{\text{ZPE}} + \Delta G_{\text{vib}} + \Delta G_{\text{trans}} + \Delta G_{\text{rot}}$$
 (3)

Geometry optimization calculations were performed to find stable ground states, which maximized adsorbate interactions with BA while minimized steric constraints imposed by the pore walls. Several different starting configurations of the hydrocarbons were considered to ensure that a significant energetic minimum was identified. As in our previous paper, chemical accuracy was ensured by comparing monomer experimental enthalpies to DFT-calculated BE, and ZPE-corrected energies were found to show the best agreement. The calculated state function values were observed to deviate from experiments in the order of ~15 kJ/mol. The same procedure for calculating BE is also used in this study. Calculating Gibbs free energies for the

adsorbed hydrocarbons is difficult. Previous studies have reported that the harmonic oscillator approximation for the normal vibrational modes of adsorbates and the zeolite framework atoms may result in poor estimates of entropic losses. ^{22,40,41} Thus, ΔG values can be found in the Supporting Information (Tables S1–S5). The calculated adsorption free energy values likely deviate from experimental values at finite temperatures, and therefore, $\Delta E_{\rm ZPE}$ will be used as the computational measure of adsorption energies to benchmark calculations.

A total of 32 pairs of adsorption energies of various hydrocarbon combinations were compared for C2-C6 alkenes and corresponding alkanes. Correlations were developed relating the carbon number to adsorption energy for alkanealkane, alkane-alkene, and alkene-alkene adsorption pairs through linear regression. R^2 and mean absolute error (MAE) are used to quantify the fit of the regression. Absolute error values can be found in the Supporting Information. Alkenealkene adsorption behavior was further examined with the additional variable of branching. Twenty-four alkene-alkene pairs were used to compare a single-variable linear regression, relating the carbon number to adsorption ZPE against a multivariable linear regression relating the carbon number and the number of branches to adsorption energy. Regressions were performed using the scikit-learn LinearRegression package⁴² in Python; the regression code can be found in the Supporting Information. To compare regression trends, three alkenealkene points were used for validation. Once again, R^2 and MAE are used and absolute error values can be found in the Supporting Information. Finally, complexes of up to six adsorbate molecules of the same identity, as well as mixtures of adsorbates, were added to the unit cell to calculate the differential adsorption energies at high concentrations or high loadings.

■ RESULTS AND DISCUSSION

Adsorption of Linear α -Alkene—Alkane Hydrocarbons at Various Acid Sites of H-ZSM-5. The adsorption behavior of linear α -alkene—alkane hydrocarbons of the same carbon number at the T7, T9, and T12 positions was first assessed (Figure 2). Any of the four oxygens bonded to Al could hold the acidic H⁺. Earlier theoretical studies have suggested that the

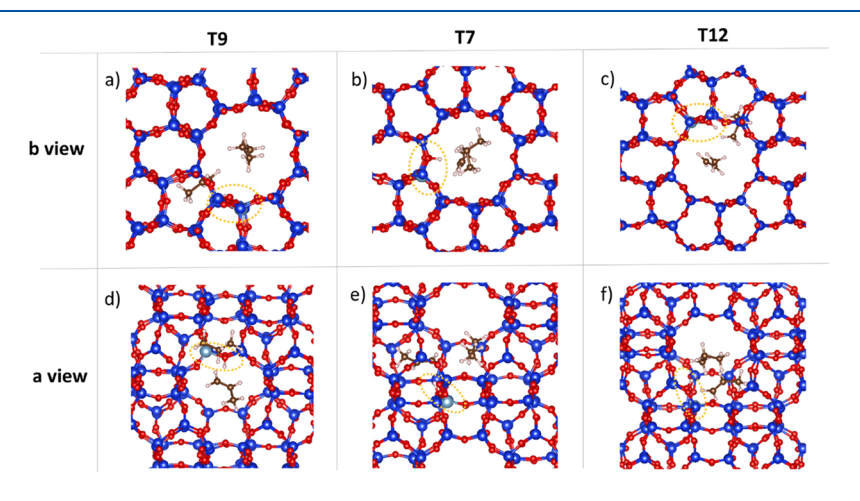


Figure 2. Graphical representation of propene—propane heterodimers at the (a and d) T9, (b and e) T7, and (c and f) T12 acid site locations in H-ZSM-5. The acid site is circled in a dashed yellow line for easier identification. "b view" shows down the channels of H-ZSM-5, and "a view" depicts the cages of H-ZSM-5.

Table 1. Adsorption Thermochemistry Values Calculated for Linear Alkene—Alkane Hydrocarbons of the Same Carbon Number at Various H-ZSM-5 T-Sites^a

		T7			Т9			T12	
species	ΔE_0	$\Delta E_{ m ZPE}$	ΔH	ΔE_0	$\Delta E_{ m ZPE}$	ΔH	ΔE_0	$\Delta E_{ m ZPE}$	ΔΗ
ethene-ethane	-96.4	-84.0	-127.3	-104.5	-91.1	-133.4	-95.0	-81.7	-124.9
propene-propane	-142.8	-129.4	-184.9	-147.0	-133.2	-188.0	-138.3	-123.7	-178.4
1-butene-butane	-158.1	-144.7	-214.2	-189.0	-176.5	-244.6	-156.3	-138.1	-204.9
1-hexene-hexane	-224.5	-208.8	-304.8	-240.9	-228.1	-324.1	-205.5	-188.2	-283.4
^a Values are reported in	n kJ/mol.								

proton can occupy the different oxygens of the tetrahedral Al site within the zeolite framework, with low energy barriers for "hopping" between the different oxygen sites. ^{43,44} Similar to the T-site, the proton was placed on the oxygen most accessible to the pore void and channels, corresponding to the lowest energy state.

The lowest energy positions for different alkene—alkane mixtures at each T-site are shown in Figure 2 and tabulated in Table 1. Linear scaling correlations between BE (BE, kJ/mol) and the alkene—alkane carbon number (ethene—ethane, propene—propane, 1-butene—butane...) are reported to better estimate dimer BEs across the different T-sites, shown in eqs 4—6 and seen in Figure 3. Generally, longer hydrocarbons will

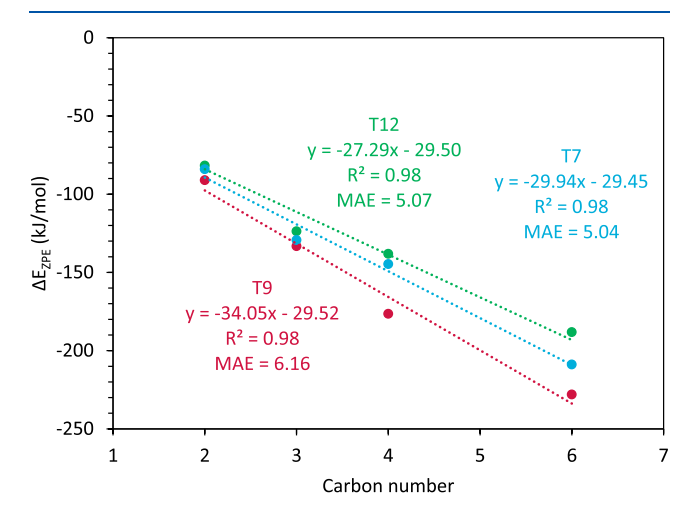


Figure 3. Calculated $\Delta E_{\rm ZPE}$ BE values of linear α -alkene—alkane adsorptions of the same carbon length (ethene—ethane, propene—propane, and 1-butene—butane) for the T12 (green), T7 (blue), and T9 (red) acid positions in H-ZSM-5. Values can be found in Table 1. Absolute errors can be found in Table S2.

bond more strongly than shorter hydrocarbons as the number of weak interactions, such as vdW forces, increases with the increasing hydrocarbon length.

$$BE_{alkene-alkane,T7} = -29.9 \times C_N - 29.5 \tag{4}$$

$$BE_{alkene-alkane,T9} = -27.3 \times C_N - 29.5 \tag{5}$$

$$BE_{alkene-alkane,T12} = -34.0 \times C_N - 29.5 \tag{6}$$

Each trend has very similar *y*-intercepts, as each T-site contains an acid site capable of bonding, theoretically, with a very small adsorbate (as the carbon number approaches 0). Likewise, at small carbon numbers, the effect of the T-site position appears minimal. All three acid sites were calculated to have almost identical ethene—ethane BE ($E_{\rm ZPE}$) of about -86 ± 5 kJ/mol. However, as the carbon number increases, the T-site position becomes more significant, as seen in the differing slope. The T-site location controls how longer adsorbates fit in the framework. At the point of hexene—hexane, the BE across the sites range from -188 to -228 kJ/mol for the T12 and T9 sites, respectively (Table 1).

To note, the T9 site exhibited the strongest binding across the alkene—alkane dimer adsorptions. This is likely due to the acid site being ideally positioned at the intersection of channels and with access to a cage. In turn, this implies that the T9 pore location provides a more ideal geometric structure to adsorb dimer hydrocarbons. Hydrocarbons have room to favorably orient with the acid site as well as room for both adsorbates to maximize interactions with the pore wall. Thus, moving forward in studying additional heterodimer adsorption events, the T9 site will be the site used for calculations.

Adsorption of the α -Alkene–Alkane Heterodimer Compared to Homodimer Adsorption. In our previous study, homodimer adsorption trends at the T9 H-ZSM-5 site were compiled, and linear correlations as a function of carbon number were reported. Comparing these previous homodimer alkane–alkane and alkene–alkene physisorption energies, the

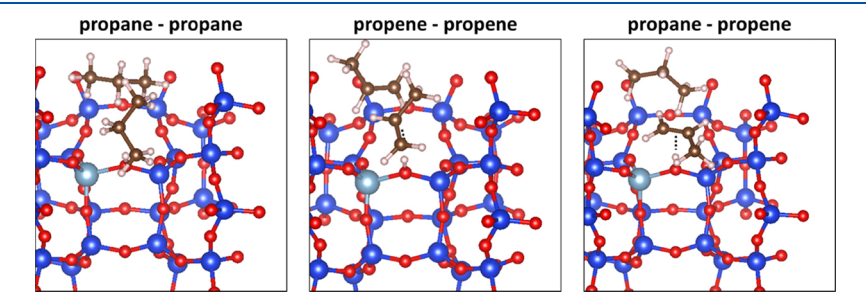


Figure 4. Graphical representation of homodimers (propane—propane and propene—propene) from a previous study compared to the α -alkene—alkane heterodimer (propene—propane) at T9 in H-ZSM-5. As seen in the propane—propene case, the double bond of the alkene orients with the proton of the acid site for the most favorable adsorption. The alkene-acid π -complex is indicated with the black dashed line.

alkene—alkane heterodimer closely follows the alkene—alkene homodimer adsorption trends (Figures 4 and 5).

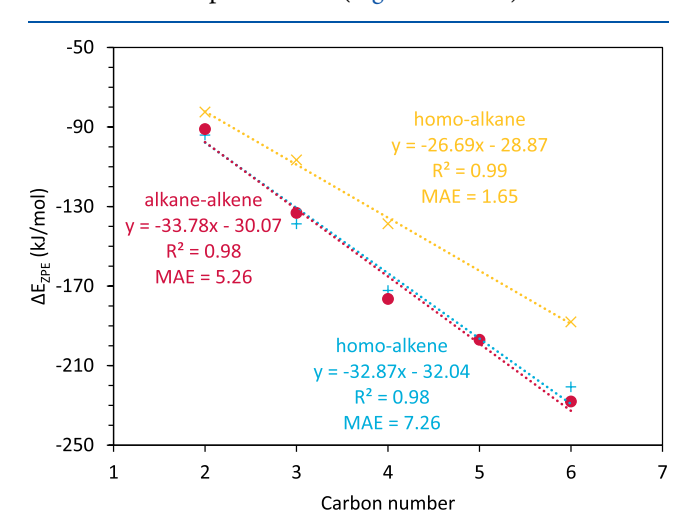


Figure 5. Calculated $\Delta E_{\rm ZPE}$ BE values for linear homodimer alkane (yellow), linear homodimer α -alkene (blue), and linear heterodimer α -alkene—alkane (red) adsorptions of the same carbon length (ethene—ethane; propene—propane, 1-butene—butane...) in H-ZSM-5.

As found previously, all the *y*-intercepts are about equal. As mentioned in the previous section, each T-site contains an acid site capable of bonding with a very small (as the carbon number goes to zero) adsorbate.

The close agreement of the BE between alkene-alkene and alkene-alkane dimers, seen in very similar regressed slopes, is likely due to the presence of the alkene C=C double bond interacting with the acid site, which can make a π -complex and adsorb more strongly than alkanes. In the heterodimer alkenealkane adsorptions, the alkene will orient itself to make such a complex, allowing the π -electrons of the C=C double bond to interact with the H acid proton (Figure 5). The very similar energies of the alkene-alkene and alkene-alkane dimers suggest that the alkene interaction is the dominating feature, while the second coadsorbed species maximizes weak favorable interactions with the framework, regardless of whether a second double bond is present. Homoalkanes, which have no alkenes present to make a stronger π -complex or π -bonds, adsorb less strongly, as seen by the less negative slope, compared to alkene alkene and alkene-alkane dimers.

Adsorption of Heterodimer Hydrocarbons. Various combinations of heterodimer hydrocarbons of different carbon lengths were investigated on the T9 site of H-ZSM-5. All calculated adsorption energies, enthalpies, and free energies are reported in Table 2. To summarize trends, heterodimers are grouped into three possibilities: alkene—alkene, alkene—alkane, and alkane—alkane. BE are plotted against the total combined carbon number of the adsorbates (Figures 6 and 7).

Linear scaling relations between heterodimer BE (kJ/mol) and the total carbon number (C_{Ntot}) in H-ZSM-5 are quantified in eqs 7–9.

$$BE_{alkane-alkane} = -14.0 \times C_{Ntot} - 29.1 \tag{7}$$

$$BE_{alkene-alkane} = -17.5 \times C_{Ntot} - 28.4 \tag{8}$$

$$BE_{alkene-alkene} = -18.3 \times C_{Ntot} - 27.7 \tag{9}$$

Similar to the alkene and alkane trends seen in homodimers, *y*-intercepts are about equal. Moreover, the alkane—alkane dimers

Table 2. Adsorption Thermochemistry Values Calculated for Heterodimer Hydrocarbons at the T9 Site of H-ZSM-5^a

species	ΔE_0	$\Delta E_{ m ZPE}$	ΔH	total C number	
alkene-alkene					
ethene-propene	-136.5	-122.0	-168.4	5	
ethene-2tbutene	-160.9	-145.7	-200.1	6	
ethene-2cbutene	-148.2	-132.8	-186.9	6	
ethene-1-hexene	-176.8	-162.2	-228.5	8	
ethene-2-hexene	-181.8	-166.5	-234.5	8	
2cbutene-2tbutene	-194.3	-179.5	-249.3	8	
2cbutene-isobutene	-191.0	-176.6	-244.6	8	
2tbutene-isobutene	-198.9	-183.8	-252.0	8	
2tbutene-1-pentene	-207.0	-191.8	-256.4	9	
isobutene-1-pentene	-187.7	-173.7	-236.6	9	
2tbutene-1-hexene	-229.1	-214.0	-295.9	10	
2tbutene-2-hexene	-240.8	-225.2	-308.4	10	
alkene-alkane					
ethene-ethane	-104.5	-91.1	-133.4	4	
propene-propane	-147.0	-133.2	-188.0	6	
propene-pentane	-180.4	-166.6	-225.6	8	
1-butene-butane	-189.0	-176.5	-244.6	8	
2cbutene-butane	-183.0	-169.3	-239.2	8	
2cbutene-isobutane	-180.2	-166.9	-236.7	8	
2tbutene-butane	-190.1	-176.0	-246.1	8	
2tbutene-isobutane	-192.6	-178.9	-248.7	8	
isobutene-isobutane	-168.4	-153.9	-220.9	8	
1-pentene-pentane	-210.5	-197.0	-259.0	10	
2-hexene-butane	-228.7	-214.4	-297.8	10	
1-hexene—hexane	-240.9	-228.1	-324.1	12	
alkane-alkane					
ethane-propane	-110.3	-97.7	-149.1	5	
ethane-butane	-131.3	-118.5	-177.2	6	
ethane-hexane	-153.2	-140.0	-212.5	8	
propane-butane	-142.3	-128.0	-191.7	7	
propane-hexane	-167.3	-156.2	-235.0	9	
butane-isobutane	-150.1	-134.7	-204.4	8	
butane-pentane	-172.0	-160.7	-229.6	9	
butane-hexane	-181.6	-169.7	-255.5	10	
^a Values are reported in kJ/mol.					

have the least negative slope, meaning that these pairs adsorb the weakest, as no C=C double bond is present to create an adsorbed π -complex. Alkene—alkane adsorption is the next strongest adsorption group, with alkene—alkene adsorption slightly stronger. As mentioned in discussing homodimer trends, alkene—alkane and alkene—alkene dimer adsorptions are reported to be very similar; both have the energy-dominant feature of aligning the double bond π -electrons, while the second adsorbate maximizes weak interactions with the framework. Thus, the alkene—alkane and alkene—alkene linear correlations can be grouped into one equation (eq 10).

$$BE_{alkene-hydrocarbon} = -17.7 \times C_{Ntot} - 29.9 \tag{10}$$

The DFT-calculated adsorption energies for n-alkanes as a function of carbon number were found to slightly over-bind relative to the force-field-based predictions by Calero et al., as well as the experimental literature. Specifically, the calculated $\Delta E_{\rm ZPE}$ values for ethene, ethane, and propane were -59, -47, and -54 kJ/mol, as compared to the experimental values of -54, -43, and -44 kJ/mol, respectively.

Interestingly, within the heterodimer adsorption group, identical total carbon numbers have adsorption energies that

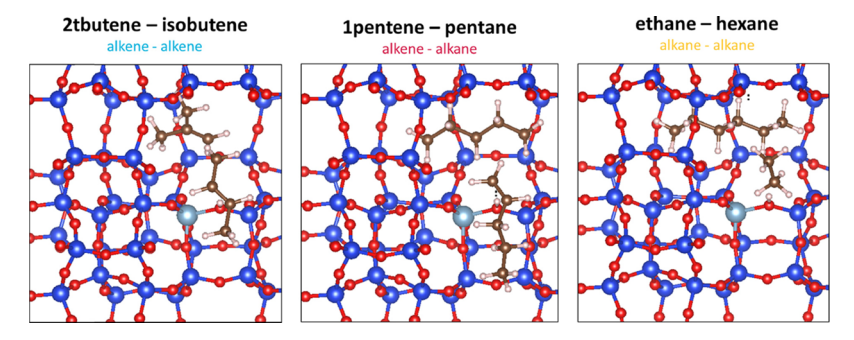


Figure 6. Graphical representation of some of the heterodimers used in this study. Heterodimers were grouped as alkene—alkene (e.g., 2-trans-butene and iso-butene), alkene—alkane (e.g., 1-pentene and pentane), and alkane—alkane (e.g., ethane—hexane) pairs. The alkene-acid π -complex is indicated with the black dashed line.

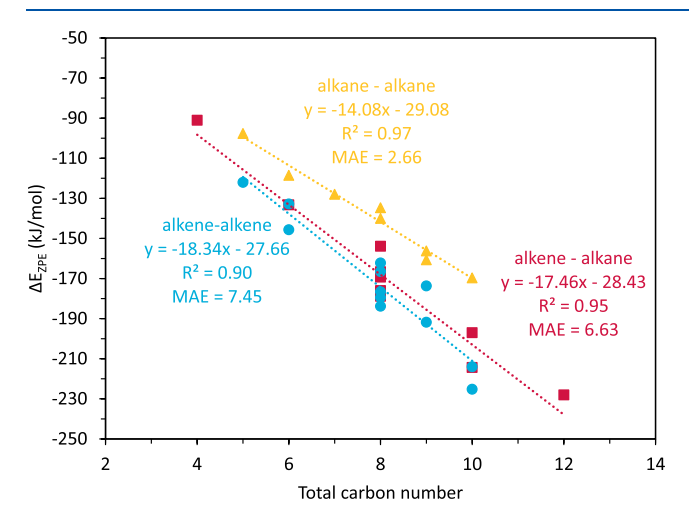


Figure 7. Calculated $\Delta E_{\rm ZPE}$ BE values for alkane—alkane (yellow), alkene—alkane (red), and alkene—alkene (blue) heterodimer adsorption for the combined carbon number of both adsorbates in H-ZSM-5. Values can be found in Table 2. Absolute errors can be found in Table S3.

are very similar. For example, propane—hexane and butane—pentane (alkane—alkane) heterodimers both have a total carbon number of 9 and have BE of -156 and -161 kJ/mol, respectively. Likewise, propene—pentane and 2-cis-butene—isobutane (alkene—alkane) both had calculated BE of -167 kJ/mol.

One source of spread of adsorption energies for each total carbon number is steric hindrance. Longer adsorbates often have steric constraints that smaller adsorbates do not, which leads to varying adsorption numbers for the same number of carbons. For example, heterodimer pairs that include one large adsorbate, like hexene or hexane, and a small adsorbate pair will generally absorb weaker than pairs that have two similarly sized adsorbates. The adsorption energy for ethene-1-hexene (C8 total) is -162 kJ/mol compared to -179 kJ/mol of 2-cisbutene-2-trans-butene (C8 total). Another source of spread is the degree of branching. For example, the weakest C8 alkenealkane adsorption at -154 kJ/mol is isobutene-isobutane, while linear combinations of butene-butanes as well as propene-pentane are much closer to the average of -172 kJ/ mol. The alkene-alkene heterodimer group contained the most branched species and may account for low R² and high MAE values compared to the other heterodimer groups. Further investigation into the effect of branching on adsorption,

specifically on the alkene-alkene group, is discussed in the next section.

Adsorption of Linear and Branched Alkenes. Further investigation was done to compare linear and branched alkene—alkene pairs, specifically focusing on linear and branched butenes and pentenes (Figure 8). All calculated adsorption energies and enthalpies are reported in Table 3.

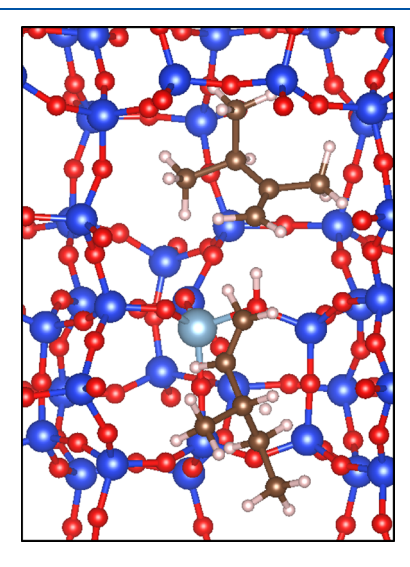


Figure 8. Graphical representation of 3-methyl-1-butene and 2,3-dimethyl-1-butene in H-ZSM-5.

Comparing the linear regression of predominately linear alkene pairs, the addition of branched alkene pairs leads to a less negative slope between BE with respect to the total carbon number (Figure 9, eq 11). Moreover, while the coefficient of the determination value of mostly linear alkene pairs was about 0.90 and the MAE was about 7.45, this linear correlation is slightly worse at describing highly branched alkene pairs with a decreased coefficient of a determination value of 0.83 and MAE of about 9.03 (Figure 9). Generally, more linear pairs adsorb more strongly than branched pairs of the same number of carbons; for example, linear 2-trans-butene-1-pentene (C9, no branches) has an adsorption energy of -191.8 kJ/mol compared to 181.8 kJ/mol for 2-trans-butene-3-methyl-1-butene (C9, 1 branch) and 164.6 kJ/mol for isobutene-3-methyl-1-butene (C9, 2 branches). More linear adsorbates likely can orient and fit within the channels of H-ZSM-5, while branched species are likely limited by sterics of these channels, destabilizing their binding.

Table 3. Adsorption Thermochemistry Values Calculated for Linear and Branched Heterodimer Alkene—Alkenes at the T9 Site of H-ZSM-5^a

species	ΔE_0	$\Delta E_{ m ZPE}$	ΔH	total C number	total branches
ethene-propene	-136.5	-122.0	-168.4	5	0
ethene-2tbutene	-160.9	-145.7	-200.1	6	0
ethene-2cbutene	-148.2	-132.8	-186.9	6	0
ethene-1-pentene	-161.0	-146.4	-195.6	7	0
ethene-2-pentene	-173.7	-159.0	-210.2	7	0
ethene—2-methyl-1- butene	-167.3	-155.2	-204.8	7	1
ethene—2-methyl-2- butene	-133.0	-142.5	-195.5	7	1
ethene—3-methyl-1- butene	-157.4	-144.8	-194.4	7	1
ethene-1-hexene	-176.8	-162.2	-228.5	8	0
ethene-2-hexene	-181.8	-166.5	-234.5	8	0
2cbutene-2tbutene	-194.3	-179.5	-249.3	8	0
2cbutene-isobutene	-191.0	-176.6	-244.6	8	1
2tbutene-isobutene	-198.9	-183.8	-252.0	8	1
ethene—3-methyl- pentene*	-175.4	-164.0	-220.5	8	1
ethene-2,3-dimethyl- butene*	-177.0	-164.1	-220.4	8	2
2tbutene-1-pentene	-207.0	-191.8	-256.4	9	0
2tbutene—2-methyl-1- butene	-204.9	-191.0	-255.3	9	1
2tbutene—2-methyl-2- butene	-203.3	-189.7	-256.3	9	1
2tbutene—3-methyl-1- butene	-195.9	-181.8	-246.3	9	1
isobutene-1-pentene	-187.7	-173.7	-236.6	9	1
isobutene-2-pentene	-206.2	-190.8	-255.0	9	1
isobutene-2-methyl-1- butene	-187.7	-172.1	-233.5	9	2
isobutene-2-methyl-2- butene	-192.1	-179.1	-244.6	9	2
isobutene-3-methyl-1- butene	-179.6	-164.6	-226.8	9	2
2tbutene-1-hexene	-229.1	-214.0	-295.9	10	0
2tbutene-2-hexene	-240.8	-225.2	-308.4	10	0
3-methyl-1-butene-2,3- dimethyl-1-butene*	-250.0	-191.2	-256.4	11	3

^aSpecies indicated by * were not used in the linear regression and serve as validation points; these species are noted in orange in Figures 6 and 7. Values are reported in kJ/mol.

Validation pairs, not used in the linear regression, are marked in orange in Figure 6. The single variable linear regression does predict the BE of ethene—3-methyl-1-pentene (C8, 1 branch) and ethene—2,3-dimethyl-1-butene (C8, 2 branches) well. However, it very poorly predicts a BE of —221.5 kJ/mol for 3-methyl-1-butene—2,3-dimethyl-1-butene (C11, 3 branches) when a binding of —191.2 kJ/mol was calculated.

$$BE_{alkene-alkene} = -17.3 \times C_{Ntot} - 31.8$$

 $R^2 = 0.829, MAE = 9.03$ (11)

To better account for a weaker adsorption with the increasing number of branches, a new multivariable linear regression was performed in Python using scikit-learn LinearRegression⁴² that considered both the total carbon number and total number of branches (Figure 10, eq 12, additional angles in the Supporting Information). Considering both variables, the coefficient of the determination value increased to 0.89, the MAE decreased to

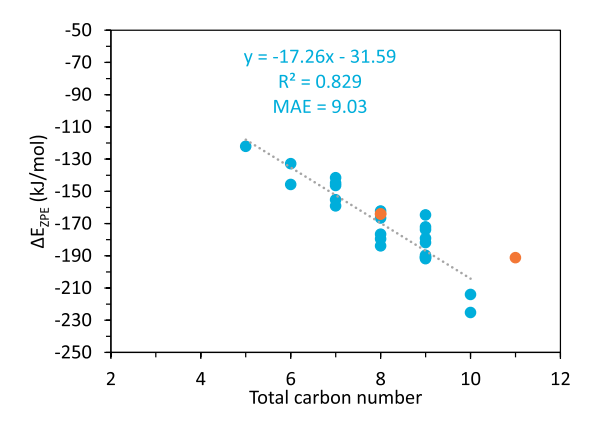


Figure 9. Calculated $\Delta E_{\rm ZPE}$ BE values and regression line for branched alkene—alkene heterodimer adsorption considering only the carbon number of both adsorbates in H-ZSM-5. $C_{\rm Ntot}$ is the total number of carbons. Blue points are points used in the linear regression, while orange markers serve as validation points. Absolute errors can be found in Table S4.

6.88, and overall, this multivariable regression better describes the trends of stronger and more negative adsorption associated with a higher total carbon number and an energy penalty for the degree of branching.

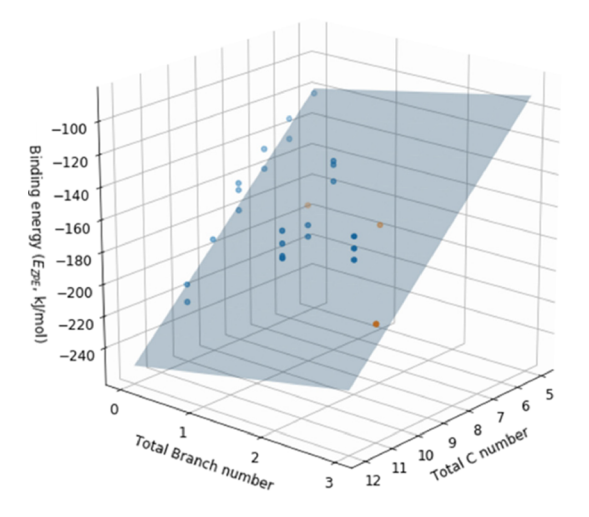
$$BE_{alkene-alkene} = -19.0 \times C_{Ntot} + 9.30 \times B_{Ntot} - 24.0$$

 $R^2 = 0.891, MAE = 6.88$ (12)

Additionally, this multivariable linear regression predicts the adsorption energy of the three validation points much more accurately. The single-variable regression predicted -169.7 kJ/ mol for both ethene-3-methyl-1-pentene (C8, 1 branch) and ethene-2,3-dimethyl-1-butene (C8, 2 branches). The multivariable linear regression predicts -166.7 and -157.4 kJ/mol, respectively, which is much closer to the calculated adsorption of about -164 kJ/mol. Moreover, the multivariable linear regression predicts a BE of -205.1 kJ/mol for the long and highly branched 3-methyl-1-butene-2,3-dimethyl-1-butene (C11, 3 branches, Figure 9). This is only about a 14 kJ/mol difference from the calculated value and a much better improvement than the 30 kJ/mol difference between the single-variable regression and the calculated value. Thus, using adsorption trends that take into account both of these variables may lead to more accurate predictions, which may be highly applicable to kinetic models.

Adsorption of Multiple Hydrocarbons. At high pressures, concentrations, or high loadings, the possibility for multiple species, more than two, to adsorb near an acid site increases. Small alkenes and alkanes (C2 and C3) were used to calculate the adsorption energies for multiadsorption events (Figures 11 and 12). Because only linear hydrocarbons were used for this section of the study, only molecular identity and the total carbon number were considered when performing linear regression.

Linear scaling relations between multiadsorbate BE (kJ/mol) and the total carbon number ($C_{\rm Ntot}$) in H-ZSM-5 are quantified in eqs 13 and 14. To note, when no *y*-intercept was set for the regression, the regressed *y*-intercepts were much less negative and inconsistent with what was previously being calculated. These original fits can be found in Figure S1. Despite having a lower MAE and comparable R^2 value, the linear trends of eqs 13 and 14 have set *y*-intercepts more consistent than those used in



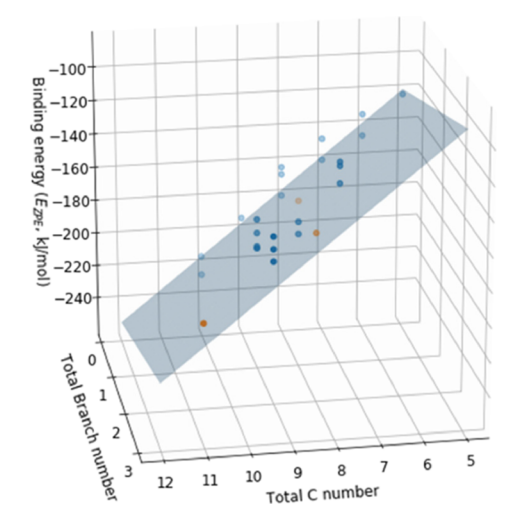


Figure 10. Calculated $\Delta E_{\rm ZPE}$ BE values and regression for branched alkene—alkene heterodimer adsorption considering both the carbon number and total number of branches of both adsorbates in H-ZSM-5. Both figures show the same data, viewed at two different angles, and another can be found as Figure S1 in the Supporting Information. $C_{\rm Ntot}$ is the total number of carbons, and $B_{\rm Ntot}$ is the total number of branches. Blue points are points used in the linear regression, while orange markers serve as validation points. Corresponding values are reported in Table 3. Absolute errors can be found in Table S4.

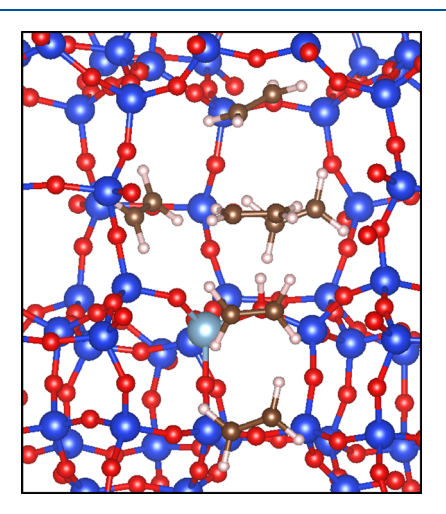


Figure 11. Graphical representation of six adsorbed ethene molecules near an H-ZSM-5 acid site.

Figure 7 and reported in eqs 7–10 (about 30 ± 2 kJ/mol) for better comparison.

$$BE_{alkane-only} = -18.6 \times C_{Ntot} - 31.5 \tag{13}$$

$$BE_{alkene(s)} = -15.8 \times C_{Ntot} - 28.0 \tag{14}$$

Previously, we found that in the presence of hydrocarbon dimers, the adsorption energy will increase linearly with the total carbon number. Using mixtures of alkenes and alkanes, this trend was found to hold past two adsorbates but also for three to six and possibly more adsorbates. Markedly, even the adsorption of a mixture of ethane, ethene, propane, and propene was found to closely follow the trend made by multiple adsorptions of the same species, suggesting an adsorption trend based on the total carbon number of all adsorbates, rather than specific hydrocarbon identity.

Once again, adsorbate mixtures of just alkanes adsorbed less strongly than mixtures with at least one alkene present, as seen in the less negative slope. This again reinforces the idea that the alkene will make a favorable π -complex with the acid site and

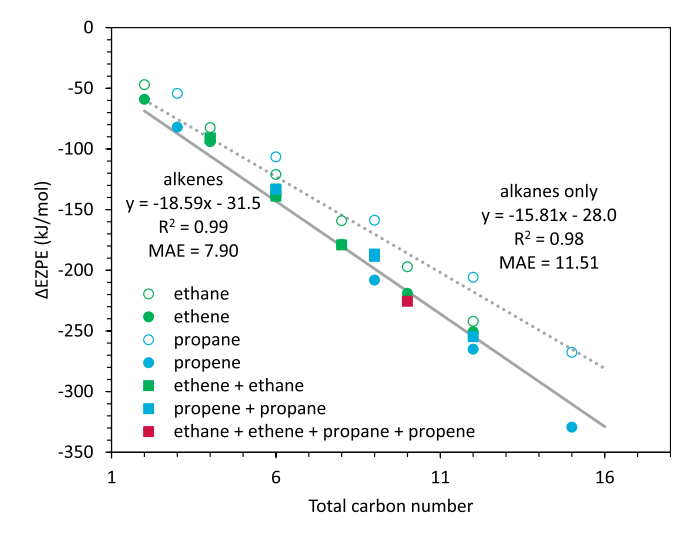


Figure 12. Calculated $\Delta E_{\rm ZPE}$ BE values for multiple adsorbates with respect to the total adsorbate carbon number in H-ZSM-5. Green open circles are the adsorption trend of adding ethane, green solid circles are the adsorption trend of adding propane, blue open circles are the adsorption trend of adding propane, blue solid circles are the adsorption trend of adding propene, green solid squares are the adsorption of mixtures of ethene and ethane, blue solid squares are the adsorption of mixtures of propene and propane, and red solid squares are the adsorption of a mixture of ethane, ethene, propane, and propene. Values can be found in Table 4. Absolute errors can be found in Table S5. *Y*-intercepts were set according to eqs 7–9.

other π -bonds, while the remaining adsorbate(s) maximize weak favorable interactions with the framework, without much significance to hydrocarbon identity (Figure 12). For example, a propane-3× adsorption has a BE of -158.8 kJ/mol. Replacing one propane with a propene gives a stronger BE of -186.7 kJ/mol for propene—propane-2×. Replacing another propane with propene only slightly strengthens the adsorption event, with a calculated BE of 188.6 kJ/mol for the propene-2×—propane complex. The strongest adsorption behavior could still be attributed to a pure alkene mixture, with a trimer of propene adsorbing the strongest at -208.1 kJ/mol (Table 4).

Table 4. Adsorption Thermochemistry Values Calculated for Multiple Hydrocarbon Adsorptions at the T9 Site of H-ZSM- S^a

species	ΔE_0	ΔE_{ZPE}	ΔH
alkene			
ethene-2×	-107.4	-94.1	-134.1
ethene-3×	-155.6	-139.1	-202.5
ethene-4×	-199.2	-178.6	-264.6
ethene-5×	-242.4	-219.0	-328.5
ethene-6×	-277.2	-250.6	-383.3
propene-2×	-152.9	-138.7	-191.8
propene-3×	-226.9	-208.1	-290.5
propene-4×	-288.3	-265.1	-377.0
propene-5×	-355.7	-329.4	-471.5
alkene-alkane			
ethene-ethane	-97.0	-84.7	-127.9
ethene-ethane-2×	-149.9	-133.2	-201.4
ethene-2×-ethane	-155.1	-139.0	-205.2
ethene-2×-ethane-2×	-197.5	-179.2	-271.6
propene-propane	-147.04	-133.24	-188.02
propene-propane-2×	-204.1	-186.7	-272.5
propene-2×-propane	-206.8	-188.6	-272.9
propene-2×-propane-2×	-274.5	-254.8	-371.3
ethene-ethane-propene-propane	-244.7	-225.6	-329.7
alkane			
ethane-2×	-93.9	-82.5	-129.2
ethane-3×	-136.3	-121.1	-192.7
ethane-4×	-179.3	-159.2	-255.9
ethane-5×	-221.3	-197.1	-319.2
ethane-6×	-268.3	-242.1	-390.5
propane-2×	-118.5	-106.6	-164.8
propane-3×	-176.4	-158.8	-246.5
propane-4×	-228.6	-205.8	-324.2
propane-5×	-292.4	-267.7	-417.9

 a^{n} "× indicates that n adsorbates were used in the calculation. Values are reported in kJ/mol. Absolute error can be found in Table S5.

Moreover, the fact that the slopes for the alkene mixture and alkane-only mixture are different and not just the intercept may indicate continuous alkene—alkene and alkene—alkane interactions with the carbon number. If the favorable π -complex with the acid site was the only difference between the alkene mixture and alkane-only mixtures, this initial and largely one-time event would likely alter the intercept alone. The difference in the slope as the total carbon number increases points to continued favorable adsorption as the carbon length is added and is likely in the form of π -stacking.

To note, only small adsorbates were used in this analysis, and as discussed in the previous section, longer adsorbates often have steric constraints, such as branching, which leads to varying adsorption numbers for the same number of carbons. Thus, the alkene-hydrocarbon slope found in this analysis is slightly more negative ($-18.6 \, \text{kJ/mol}$) than the slope reported in the previous section. Likewise, the R^2 value is higher and MAE is lower for the analysis of only small adsorbates compared to heterodimer pairs with larger adsorbates as the small adsorbates are free from the steric constraints that would weaken the adsorption. Despite this small difference in the BE slope, the trends of dimer pairs are very close (about $\pm 1 \, \text{kJ/mol}$) to the trends of multiple adsorbates. Thus, the trends found for alkene and alkane heterodimers may also accurately extend to multiple larger adsorbates (>C3+ at high loadings) near a single acid site as well.

CONCLUSIONS

Adsorption into acidic zeolites is a crucial first step in industrial processes that are widely used, including catalytic reactions and molecular separations. In this work, we address the gap in understanding of how mixtures of dimers and multiple species adsorb into the zeolite, which is relevant for bimolecular reactions or hydrocarbon separations. The systems were analyzed, and the significant conclusions are as follows:

- i. Electronic energies, enthalpies, and free energies of adsorption were calculated for linear α -alkene—alkane dimers at various acid sites of H-ZSM-5, which suggested that the T9 site was ideally situated for favorable adsorptions for heterodimers. Hydrocarbon adsorbates want to ideally sit within the channels of the pore, and an acid site location more available at these positions leads to stronger binding.
- ii. Linear α -alkene—alkane heterodimer energies were compared against homodimer energies, and the dominating influence of the alkene in adsorption was revealed. In the presence of at least one alkene, BE were found to be much stronger and more negative, likely due to the presence of more powerful π -bonding.
- iii. Adsorption energies for a variety of dimer species were quantified, and class-specific linear scaling relations were developed for estimating adsorption as a function of total combined carbon numbers of both adsorbates. Again, the dominating effect of the alkene presence greatly increases bonding strength, as seen by the more negative slope of alkene pairs compared to alkane-only pairs.
- iv. Further investigation into linear and branched alkene—alkene pairs led to the development of a multivariable linear correlation, relating the total carbon number and the total branch number to adsorption energy. The multivariable regression more accurately predicted BE, suggesting that sterics and the branching degree, not just the carbon length alone, play an important role in how adsorbates fit into the channels of H-ZSM-5 and how strongly adsorbates bind.
- v. Linear trends were found to hold past two adsorbates, for multispecies systems of up to six adsorbates as well. The slopes of these linear trends also closely match those found for dimer species, suggesting that the linear scaling relationships could be extended to predict many large adsorbates near acid sites (high loadings).

The findings reported in this work provide advancements of existing linear scaling relations and add to the accuracy of mixed feed models. The reported adsorption trends are highly versatile and industrially relevant in application to catalyzed reactions and molecular sieves.

ASSOCIATED CONTENT

Supporting Information

The Supporting Information is available free of charge at https://pubs.acs.org/doi/10.1021/acs.jpcc.2c02610.

Gibbs free energy, absolute errors, linear regression of multiple adsorbates with set *y*-intercepts, and the Python code for multivariable linear regression (PDF)

AUTHOR INFORMATION

Corresponding Author

Linda J. Broadbelt — Department of Chemical and Biological Engineering, Northwestern University, Evanston, Illinois 60208, United States; ⊙ orcid.org/0000-0003-4253-592X; Email: broadbelt@northwestern.edu

Authors

Elsa Koninckx — Department of Chemical and Biological Engineering, Northwestern University, Evanston, Illinois 60208, United States; Orcid.org/0000-0002-2261-9782

Pavlo Kostetskyy — Department of Chemical and Biological Engineering, Northwestern University, Evanston, Illinois 60208, United States; Orcid.org/0000-0003-2796-0362

Complete contact information is available at: https://pubs.acs.org/10.1021/acs.jpcc.2c02610

Notes

The authors declare no competing financial interest. All coordinates corresponding to the converged ground states can be found at https://doi.org/10.5281/zenodo.6407225.

ACKNOWLEDGMENTS

This paper is based upon work supported primarily by the National Science Foundation (NSF) GRFP Grant DGE-1842165 and under Cooperative Agreement No. EEC-1647722 and the Belgium American Education Fellowship (BAEF). This research was also supported through the computational resources and staff contributions provided for the Quest high performance computing facility at Northwestern University, which is jointly supported by the Office of the Provost, the Office for Research, and Northwestern University Information Technology. This work used the Extreme Science and Engineering Discovery Environment (XSEDE), which is supported by National Science Foundation grant number ACI-1053575.

REFERENCES

- (1) Weitkamp, J. Zeolites and Catalysis. Solid State Ionics 2000, 131, 175–188.
- (2) Barthomeuf, D. Basic Zeolites: Characterization and Uses in Adsorption and Catalysis. *Catal. Rev. Sci. Eng.* **1996**, 38, 521–612.
- (3) Li, Y.; Li, L.; Yu, J. Applications of Zeolites in Sustainable Chemistry. *Chem* **2017**, *3*, 928–949.
- (4) Maxwell, I. E. Nonacid Catalysis with Zeolites. *Adv. Catal.* **1982**, 31, 1–76.
- (5) Auerbach, S. M.; Carrado, K. A.; Dutta, P. K. Handbook of Zeolite Science and Technology; Marcel Dekker, Inc.: New York, 2003.
- (6) Jacobs, P. A.; Martens, J. A. Introduction to Acid Catalysis with Zeolites in Hydrocarbon Reactions. *Stud. Surf. Sci. Catal.* **1991**, *58*, 445–496.
- (7) Soscún, H.; Castellano, O.; Hernández, J. Adsorption of CH₃SH in Acidic Zeolites: A Theoretical Study. *J. Phys. Chem. B* **2004**, *108*, 5620–5626.
- (8) Jones, A. J.; Iglesia, E. The Strength of Brønsted Acid Sites in Microporous Aluminosilicates. *ACS Catal.* **2015**, *5*, 5741–5755.
- (9) Zhang, N.; Liu, C.; Ma, J.; Li, R.; Jiao, H. Determining the Structures, Acidity and Adsorption Properties of Al Substituted HZSM-5. *Phys. Chem. Phys.* **2019**, *21*, 18758–18768.
- (10) Alvarado-Swaisgood, A. E.; Barr, M. K.; Hay, P. J.; Redondo, A. Ab Initio Quantum Chemical Calculations of Aluminum Substitution in Zeolite ZSM-5. *J. Phys. Chem.* **1991**, *95*, 10031–10036.
- (11) Smit, B.; Maesen, T. L. M. Molecular Simulations of Zeolites: Adsorption, Diffusion, and Shape Selectivity. *Chem. Rev.* **2008**, *108*, 4125–4184.

- (12) Piccini, G.; Sauer, J. Effect of Anharmonicity on Adsorption Thermodynamics. J. Chem. Theory Comput. 2014, 10, 2479–2487.
- (13) Krukau, A. V.; Vydrov, O. A.; Izmaylov, A. F.; Scuseria, G. E. Influence of the Exchange Screening Parameter on the Performance of Screened Hybrid Functionals. *J. Chem. Phys.* **2006**, *125*, 224106.
- (14) Li, Y. P.; Bell, A. T.; Head-Gordon, M. Thermodynamics of Anharmonic Systems: Uncoupled Mode Approximations for Molecules. *J. Chem. Theory Comput.* **2016**, *12*, 2861–2870.
- (15) Göltl, F.; Hafner, J. Modelling the Adsorption of Short Alkanes in Protonated Chabazite: The Impact of Dispersion Forces and Temperature. *Microporous Mesoporous Mater.* **2013**, *166*, 176–184.
- (16) Alexopoulos, K.; Lee, M. S.; Liu, Y.; Zhi, Y.; Liu, Y.; Reyniers, M.-F. F.; Marin, G. B.; Glezakou, V. A.; Rousseau, R.; Lercher, J. A. Anharmonicity and Confinement in Zeolites: Structure, Spectroscopy, and Adsorption Free Energy of Ethanol in H-ZSM-5. *J. Phys. Chem. C* **2016**, 120, 7172–7182.
- (17) Campbell, C. T.; Sellers, J. R. V. The Entropies of Adsorbed Molecules. J. Am. Chem. Soc. 2012, 134, 18109–18115.
- (18) Sprowl, L. H.; Campbell, C. T.; Árnadóttir, L. Hindered Translator and Hindered Rotor Models for Adsorbates: Partition Functions and Entropies. *J. Phys. Chem. C* **2016**, *120*, 9719–9731.
- (19) Dauenhauer, P. J.; Abdelrahman, O. A. A Universal Descriptor for the Entropy of Adsorbed Molecules in Confined Spaces. *ACS Cent. Sci.* **2018**, *4*, 1235–1243.
- (20) Campbell, C. T.; Sprowl, L. H.; Árnadóttir, L. A. Equilibrium Constants and Rate Constants for Adsorbates: Two-Dimensional (2D) Ideal Gas, 2D Ideal Lattice Gas, and Ideal Hindered Translator Models. *J. Phys. Chem. C* **2016**, *120*, 10283–10297.
- (21) Kerber, T.; Sierka, M.; Sauer, J. Application of Semiempirical Long-Range Dispersion Corrections to Periodic Systems in Density Functional Theory. *J. Comput. Chem.* **2008**, *29*, 2088–2097.
- (22) Göltl, F.; Grüneis, A.; Bučko, T.; Hafner, J. Van Der Waals Interactions between Hydrocarbon Molecules and Zeolites: Periodic Calculations at Different Levels of Theory, from Density Functional Theory to the Random Phase Approximation and Moller-Plesset Perturbation Theory. *J. Chem. Phys.* **2012**, *137*, 204102.
- (23) Eder, F.; Lercher, J. A. Alkane Sorption in Molecular Sieves: The Contribution of Ordering, Intermolecular Interactions, and Sorption on Brønsted Acid Sites. *Zeolites* **1997**, *18*, 75–81.
- (24) Eder, F.; Stockenhuber, M.; Lercher, J. A. Brønsted Acid Site and Pore Controlled Siting of Alkane Sorption in Acidic Molecular Sieves. *J. Phys. Chem. B* **1997**, *101*, 5414–5419.
- (25) Bates, S. P.; Van Well, W. J. M.; Van Santen, R. A.; Smit, B. Energetics of N-Alkanes in Zeolites: A Configurational-Bias Monte Carlo Investigation into Pore Size Dependence. *J. Am. Chem. Soc.* **1996**, 118. 6753—6759.
- (26) Jirák, Z.; Vratislav, S.; Bosáček, V. A Neutron Diffraction Study of H, Na-Y Zeolites. *Phys. Chem. Solids* **1980**, *41*, 1089–1095.
- (27) Smith, D. G. A.; Burns, L. A.; Patkowski, K.; Sherrill, C. D. Revised Damping Parameters for the D3 Dispersion Correction to Density Functional Theory. *J. Phys. Chem. Lett.* **2016**, *7*, 2197–2203.
- (28) Grimme, S.; Ehrlich, S.; Goerigk, L. Effect of the Damping Function in Dispersion Corrected Density Functional Theory. *J. Comput. Chem.* **2011**, 32, 1456–1465.
- (29) Grimme, S.; Antony, J.; Ehrlich, S.; Krieg, H. A Consistent and Accurate Ab Initio Parametrization of Density Functional Dispersion Correction (DFT-D) for the 94 Elements H-Pu. *J. Chem. Phys.* **2010**, 132, 154104.
- (30) Czarniecki, J.; Jaroniec, M. Studies of Adsorption Kinetics by Means of the Stochastic Numerical Simulation. *Surf. Sci. Rep.* **1983**, 3, 301–353.
- (31) Vlugt, T. J. H.; Krishna, R.; Smit, B. Molecular Simulations of Adsorption Isotherms for Linear and Branched Alkanes and Their Mixtures in Silicalite. *J. Phys. Chem. B* **1999**, *103*, 1102–1118.
- (32) Snurr, R. Q.; Bell, A. T.; Theodorou, D. N. Prediction of Adsorption of Aromatic Hydrocarbons in Silicalite from Grand Canonical Monte Carlo Simulations with Biased Insertions. *J. Phys. Chem.* **1993**, *97*, 13742–13752.

- (33) Nguyen, C. M.; De Moor, B. A.; Reyniers, M. F.; Marin, G. B. Physisorption and Chemisorption of Linear Alkenes in Zeolites: A Combined QM-Pot(MP2//B3LYP:GULP)-Statistical Thermodynamics Study. J. Phys. Chem. C 2011, 115, 23831-23847.
- (34) De Moor, B. A.; Reyniers, M. F.; Gobin, O. C.; Lercher, J. A.; Marin, G. B. Adsorption of C2-C8 n-Alkanes in Zeolites. J. Phys. Chem. C 2011, 115, 1204-1219.
- (35) De Moor, B. A.; Reyniers, M. F.; Sierka, M.; Sauer, J.; Marin, G. B. Physisorption and Chemisorption of Hydrocarbons in H-FAU Using QM-Pot(MP2//B3LYP) Calculations. J. Phys. Chem. C 2008, 112,
- (36) Kostetskyy, P.; Koninckx, E.; Broadbelt, L. J. Probing Monomer and Dimer Adsorption Trends in the MFI Framework. J. Phys. Chem. B **2021**, *125*, *7*199–*7*212.
- (37) Kresse, G.; Joubert, D. From Ultrasoft Pseudopotentials to the Projector Augmented-Wave Method. Phys. Rev. B Condens. Matter Mater. Phys. 1999, 59, 1758-1775.
- (38) Kresse, G.; Furthmüller, J. Efficient Iterative Schemes for Ab Initio Total-Energy Calculations Using a Plane-Wave Basis Set. Phys. Rev. B Condens. Matter Mater. Phys. 1996, 54, 11169-11186.
- (39) Baerlocher, C.; McCusker, L. B. Database of Zeolite Structures http://www.iza-structure.org/databases/ (accessed 2020-01-24).
- (40) Piccini, G.; Alessio, M.; Sauer, J.; Zhi, Y.; Liu, Y.; Kolvenbach, R.; Jentys, A.; Lercher, J. A. Accurate Adsorption Thermodynamics of Small Alkanes in Zeolites. Ab Initio Theory and Experiment for H-Chabazite. J. Phys. Chem. C 2015, 119, 6128-6137.
- (41) Jiang, T.; Göltl, F.; Bulo, R. E.; Sautet, P. Effect of Temperature on the Adsorption of Short Alkanes in the Zeolite SSZ-13-Adapting Adsorption Isotherms to Microporous Materials. ACS Catal. 2014, 4, 2351-2358.
- (42) Pedregosa, F.; Varoquaux, G.; Gramfort, A.; Michel, V.; Thirion, B.; Grisel, O.; Blondel, M.; Prettenhofer, P.; Weiss, R.; Dubourg, V.; Vanderplas, J.; Passos, A.; Cournapeau, D.; Brucher, M.; Perrot, M.; Duchesnay, E. Scikit-Learn: Machine Learning in Python. J. Mach. Learn. Res. 2011, 12, 2825-2830.
- (43) Tuma, C.; Sauer, J. A Hybrid MP2/Planewave-DFT Scheme for Large Chemical Systems: Proton Jumps in Zeolites. Chem. Phys. Lett. **2004**, 387, 388-394.
- (44) Ryder, J. A.; Chakraborty, A. K.; Bell, A. T. Density Functional Theory Study of Proton Mobility in Zeolites: Proton Migration and Hydrogen Exchange in ZSM-5. J. Phys. Chem. B 2000, 104, 6998-7011.
- (45) Calero, S.; Lobato, M. D.; García-Pérez, E.; Mejías, J. A.; Lago, S.; Vlugt, T. J. H.; Maesen, T. L. M.; Smit, B.; Dubbeldam, D. A Coarse-Graining Approach for the Proton Complex in Protonated Aluminosilicates. J. Phys. Chem. B 2006, 110, 5838-5841.
- (46) Doelle, H. J.; Heering, J.; Riekert, L.; Marosi, L. Sorption and Catalytic Reaction in Pentasil Zeolites. Influence of Preparation and Crystal Size on Equilibria and Kinetics. J. Catal. 1981, 71, 27-40.

□ Recommended by ACS

Combining Theoretical and Experimental Methods to Probe Confinement within Microporous Solid Acid Catalysts for **Alcohol Dehydration**

Matthew E. Potter, Lindsay-Marie Armstrong, et al.

APRIL 17, 2023 ACS CATALYSIS

Untangling Framework Confinements: A Dynamical Study on Bulky Aromatic Molecules in MFI Zeolites

Yi Ji, Guangjin Hou, et al.

NOVEMBER 29, 2022

ACS CATALYSIS

READ M

Loading-Driven Diffusion Pathway Selectivity in Zeolites with Continuum Intersecting Channels

Wei Rao, Anmin Zheng, et al.

APRIL 05, 2023

THE JOURNAL OF PHYSICAL CHEMISTRY LETTERS

RFAD 17

Brønsted Acid Strength Does Not Change for Bulk and External Sites of MFI Except for Al Substitution Where **Silanol Groups Form**

Haliey Balcom, David Hibbitts, et al.

MARCH 20, 2023

ACS CATALYSIS

RFAD 🗹

Get More Suggestions >